Inorganic Chemistry

ARTICLE

pubs.acs.org/IC

CO-Induced Formation of an Interpenetrating Bicuboctahedral Au_2Pd_{18} Kernel in Nanosized $Au_2Pd_{28}(CO)_{26}(PEt_3)_{10}$: Formal Replacement of an Interior $(\mu_{12}\text{-Pd})_2$ Fragment in the Corresponding Known Isostructural Homopalladium $Pd_{30}(CO)_{26}(PEt_3)_{10}$ with Nonisovalent $(\mu_{12}\text{-Au})_2$ and Resulting Experimental/Theoretical Implications

Evgueni G. Mednikov,*,† Sergei A. Ivanov,‡ and Lawrence F. Dahl*,†

†Department of Chemistry, University of Wisconsin—Madison, Madison, Wisconsin 53706, United States

‡Center for Integrated Nanotechnologies, Los Alamos National Laboratory, Los Alamos, New Mexico 87545, United States

Supporting Information

ABSTRACT: Initially isolated from $Pd_{10}(CO)_{12}(PEt_3)_6$ (**5**) and $Au(SMe_2)Cl$ precursors in a two-step carbon monoxide (CO)-involved procedure, the nanosized interpenetrating bicuboctahedral gold (Au)−palladium (Pd) $Au_2Pd_{28}(CO)_{26}(PEt_3)_{10}$ (**1**) was then directly obtained in 25−30% yield from the CO-induced reaction of the CO-stable Au-centered cuboctahedral $Au_2Pd_{21}(CO)_{20}(PEt_3)_{10}$ (**3**) with the structurally analogous CO-unstable $Pd_{23}(CO)_{20}(PEt_3)_{10}$ (**4**). Our hypothesis that this latter synthesis is *initiated* by the reaction of **3** with coordinatively unsaturated homopalladium species resulting from *CO-induced fragmentation* of **4** was subsequently substantiated by the alternatively designed synthesis of **1** (∼25% yield) from the CO-induced reaction of **3** with the structurally dissimilar CO-unstable $Pd_{38}(CO)_{28}(PEt_3)_{12}$ (**6**). The composition of **1**, unambiguously established from a 100 K CCD X-ray diffractometry study, is in accordance with single-crystal X-ray Au−Pd field-emission microanalysis. The *pseudo*-C_{2h} 30-atom Au_2Pd_{28} geometry of **1** may be formally derived via substitution of the *interior* $(\mu_{12}\text{-Pd})_2$ moiety in the interpenetrating bicuboctahedral Pd_{20} kernel of the known isostructural $Pd_{30}(CO)_{26}(PEt_3)_{10}$ (**2**) with the corresponding *interior* $(\mu_{12}\text{-Au})_2$ moiety, in which the otherwise entire metal-core geometry and CO/PR_3-ligated environment are essentially not altered. Of major significance is that this *interior* nonisovalent Pd-by-Au replacement in **2** produces CO-stable **1**, whereas nanosized CO/PR_3-ligated homopalladium Pd_n clusters with $n > 10$ are generally unstable under CO. Because the two adjacent encapsulated Au atoms of 2.811(1) Å separation are *not* present on the metal surface, isolation of **1** under CO is ascribed to an electronic property. The virtually *ideal geometrical site-occupancy fit* between **1** and **2** provides definite crystallographic evidence for extensive delocalization in **1** of the two valence Au 6s electrons over the entire cluster (instead of a "localized" covalent Au−Au electron-pair interaction). Gradient-corrected (pseudo-scalar-relativistic) density functional theory (DFT) calculations were performed on the isostructural $Au_2Pd_{28}(CO)_{26}(PH_3)_{10}$ (**1-H**) and $Pd_{30}(CO)_{26}(PH_3)_{10}$ (**2-H**) model clusters along with hypothetical $[Au_2Pd_{28}(\mathbf{1\text{-}H})]^{2+}$ and $[Pd_{30}(\mathbf{2\text{-}H})]^{2-}$ analogues (with phosphine ethyl substituents replaced by hydrogen ones). Natural population analysis of these four model clusters revealed similar highly positively charged metal surfaces of 28 Pd atoms relative to the two negatively charged interior metal atoms, which reflect a partially oxidized metal surface due to dominant CO back-bonding. The surprising observation that each less electronegative interior Pd atom in **2-H** is more negatively charged by 0.30e than each interior Au atom in **1-H** points to a more cationic Au in **1** than interior Pd in **2**; this unexpected (opposite) charge difference is consistent with delocalization of each Au 6s valence electron toward a Au^+ configuration. This premise is in agreement with the calculated Wiberg bond index (WBI) value of 0.055 for the Au−Au bond order in **1-H** versus the WBI single-bond value of 1.01 obtained from analogous DFT calculations for the bare, neutral Au_2 dimer, which has a much shorter spectroscopically determined gas-phase distance of 2.472 Å (that corresponds to a "localized" electron-pair interaction). Isolation of **1** under CO is of prime importance in nanoscience/nanotechnology in establishing relative stabilizations toward CO in well-defined CO/PEt_3-ligated nonisovalent Pd_2-by-Au_2-substituted Au_2Pd_{n-2} clusters [namely, $n = 30$ (**1**) and 23 (**3**)]. These important stereochemical implications have a direct relevance to the recent report of the higher tolerance to CO poisoning of highly active Au−Pd nanoparticle catalysts used for the complete conversion of formic acid into high-purity hydrogen (and CO_2) for chemical hydrogen storage.

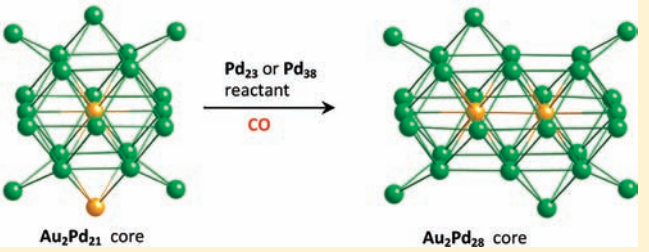

Received: September 1, 2011
Published: October 25, 2011

INTRODUCTION

Our continuing interest in the preparation and characterization of new nanosized Au−Pd carbonyl/phosphine clusters largely stems from structural/bonding and growth-pattern changes together with different reactivity behavior exhibited by the incorporation of gold into homopalladium clusters. This research is closely related to the wide variety of Au−Pd materials, especially bimetallic Au−Pd nanoparticle alloys, that are utilized mainly as precursors in Au−Pd catalysis. These particular bimetallic catalysts combining Au with Pd have been extensively investigated over the past decade, and widespread applications of Au−Pd catalysts to highly diverse chemical syntheses and fuel cells have been reported.[1,2] Prominent recent examples illustrating the complexities as well as breadth of these studies include the following: (1) direct synthesis of H_2O_2 from H_2 and O_2 via (acid-pretreated TiO_2)-supported Au−Pd catalysts;[1e] (2) carbon monoxide (CO) oxidation to CO_2 via coadsorption of both CO and atomic O (from O_2) on AuPd(100) single crystals;[1f] (3) solvent-free oxidation of alcohols to corresponding aldehydes/ketones via membrane-occluded Au−Pd nanoclusters;[1g] (4) alcohol oxidations in aqueous solutions to corresponding aldehydes/ketones via Au−Pd nanoparticle catalysts;[1h] (5) oxidation of polyethylene dodecyl ether with O_2 in H_2O to corresponding carboxylic acid via C-supported Au−Pd nanoparticles;[1i] (6) solvent-free oxidation of primary C−H bonds with O_2 in toluene via (C or TiO_2)-supported Au−Pd alloy nanoparticles;[1j] (7) development of C-supported Au−Pd catalysts for a borohydride fuel cell.[1k] Goodman and co-workers[2b] recently published a comprehensive report concerning the mechanism of the promotional effect of gold in Pd−Au alloy catalysts (with *low* Pd surface coverages) used in acetoxylation of ethylene into vinyl acetate; the commercial importance of this reaction is evidenced by the multiton production of vinyl acetate monomer through Pd-catalyzed oxidative coupling of acetic acid with ethylene.

To date, the total bimetallic (Au + Pd) nuclearity in known Au−Pd clusters is directly related to their metal-core compositions, as defined by the Au−Pd atomic ratio. Thus, for crystallographically reported Au-rich clusters (i.e., a high Au−Pd ratio) such as $([Pd(AuPPh_3)_8]^{2+}$,[3] $[Pd(CO)(AuPPh_3)_8]^{2+}$,[3] and neutral $(\mu_{12}$-$Pd)(AuPPh_3)_8(AuCl)_4)$,[4] the total nuclearity does not exceed 13, whereas for Pd-rich clusters (i.e., low Au−Pd ratio), the total bimetallic nuclearity is noticeably much higher (namely, 16−43); examples are dicationic $[Au_2Pd_{14}(CO)_9(PMe_3)_{11}]^{2+}$,[5] neutral $Au_2Pd_{21}(CO)_{20}(PR_3)_{10}$ [R = Me, Et (**3**)],[6a] and its structurally related (vide infra) and electronically equivalent monoanionic $[AuPd_{22}(CO)_{20}(PPh_3)_4(PMe_3)_6]^-$,[6a] along with three other neutral clusters, $Au_2Pd_{41}(CO)_{27}(PEt_3)_{15}$,[6b] $Au_4Pd_{28}(CO)_{22}$-$(PMe_3)_{16}$,[6c] and $Au_4Pd_{32}(CO)_{28}(PMe_3)_{14}$.[6d] The surfaces of the metal cores of these latter Pd-rich clusters typically consist of Pd atoms that are ligated by bridging COs and small-sized PR_3 groups (R = Me, Et). In contrast, the above-mentioned Au-rich clusters have Au surface atoms, with each Au atom coordinated to a triphenylphosphine ligand. One net consequence is that, in the current exploratory syntheses of nanosized Au−Pd CO/PR_3-ligated clusters, we normally use $Au(SMe_2)Cl$ [instead of $Au(PPh_3)Cl$] along with an *excess* of the palladium(0) carbonyl/trialkylphosphine precursor, which is also a prime CO source.

The two previously mentioned neutral $Au_2Pd_{21}(CO)_{20}(PR_3)_{10}$ clusters [R = Me, Et (**3**)][6a] are isostructural with the centered hexacapped cuboctahedral homopalladium $Pd_{23}(CO)_{20}(PR_3)_{10}$ [R_3 = Et_3 (**4**), Bu^n_3, Me_2Ph];[6e,7] hence, their Au_2Pd_{21} cores may be formally derived from the homopalladium Pd_{23} core via the "atomic-tweezers method" involving the Pd-by-Au replacement of both the centered and one of the six square-capped Pd atoms. The resulting triethylphosphine-ligated neutral, nonisovalent Au_2Pd_{21} cluster (**3**), which possesses two additional valence electrons relative to that in the isostructural triethylphosphine-ligated homopalladium Pd_{23} cluster (**4**), has been studied by cyclovoltammetry (CV). The CV measurements revealed that the triethylphosphine Pd_{23} cluster (**4**) undergoes one quasi-reversible two-electron reduction and two quasi-reversible one-electron oxidations,[6e,8] whereas the corresponding triethylphosphine Au_2Pd_{21} cluster (**3**) exhibits two reversible one-electron reductions and two reversible one-electron oxidations;[6a,8] the two-electron-reduced Pd_{23} cluster (**4**) corresponds to the same valence electron count as those of both neutral Au_2Pd_{21} clusters. Although both **3** and **4** undergo a net two-electron reduction and a net two-electron oxidation, their reactivities toward CO are markedly different (vide infra). Syntheses and stereochemistries of CO/PR_3-ligated nanosized Au−Pd, as well as Pd−Ni, Pd−Pt, and homopalladium clusters, are discussed in a recent review.[8]

Herein we report the synthesis, structural/spectroscopic characterization, and natural atomic population analysis by density functional theory (DFT) calculations of another remarkable CO-stable Au−Pd $Au_2Pd_{28}(CO)_{26}(PEt_3)_{10}$ (**1**). Its preparation emphasizes the importance of CO-induced reactions as a pathway to new Au−Pd clusters via initial fragmentation of large homopalladium CO/PR_3-ligated clusters under a CO atmosphere. The molecular geometry of **1** may be conceptually derived from the known isostructural geometry of the interpenetrating bicuboctahedral $Pd_{30}(CO)_{26}(PEt_3)_{10}$ (**2**)[6g,9] by substitution of the two adjacent encapsulated (μ_{12}-Pd) atoms by two nonisovalent $(\mu_{12}$-$Au)_2$ atoms. The existence of this "twinned" Au−Pd interpenetrating bicuboctahedral Au_2Pd_{18} kernel in **1** also has direct relevance to the multitwinned structures and growth patterns of larger homometallic/bimetallic clusters and naked/ligated nanoparticles.[10]

RESULTS AND DISCUSSION

Solid-State Structure of 1 and Its Close Geometrical Resemblance to 2. *a. Detailed Analysis.* Cluster **1** is isostructural with the previously isolated **2**; both possess a virtually identical *pseudo*-C_{2h} metal-core geometry with the same connectivities in CO/PEt_3 ligation. The Au_2Pd_{28} metal core in **1** (Figure 1a) is comprised of two interpenetrating Au-centered Au_2Pd_{11} cuboctahedra, which form a "twinned" 20-atom Au_2-interior Au_2Pd_{18} bicuboctahedral kernel [Au in yellow and Pd(cub) in dark green] that is capped on six of its eight square Pd_4 faces by six Pd atoms [viz., four Pd(eq) and two Pd(ap) in light green] and additionally edge-bridged by four wingtip (exopolyhedral) Pd(exo) atoms (in blue).

The 10 PEt_3 ligands in **1** (Figure 1b) and **2** (Figure 1c) are coordinated as follows: six are attached to the four Pd(eq) and two Pd(ap) atoms and the remaining four to the four Pd(exo) atoms. The analogous steric dispositions of the 26 bridging COs in both **1** and **2** consist of 22 doubly bridging μ_2-COs: of these, 10 μ_2-COs link all 10 Pd−Pd edges about the middle (equatorial) $M_2Pd(cub)_6Pd(eq)_4$ plane (M = Au in **1** and Pd in **2**), eight μ_2-COs span the eight Pd(exo)−Pd(cub) edges of the four exopolyhedral trigonally coordinated Pd(exo) atoms, and four μ_2-COs are attached to two opposite Pd(cub)−Pd(cub) edges of each of the two centrosymmetrically related noncapped

dx.doi.org/10.1021/ic201923y |*Inorg. Chem.* 2011, 50, 11795–11806

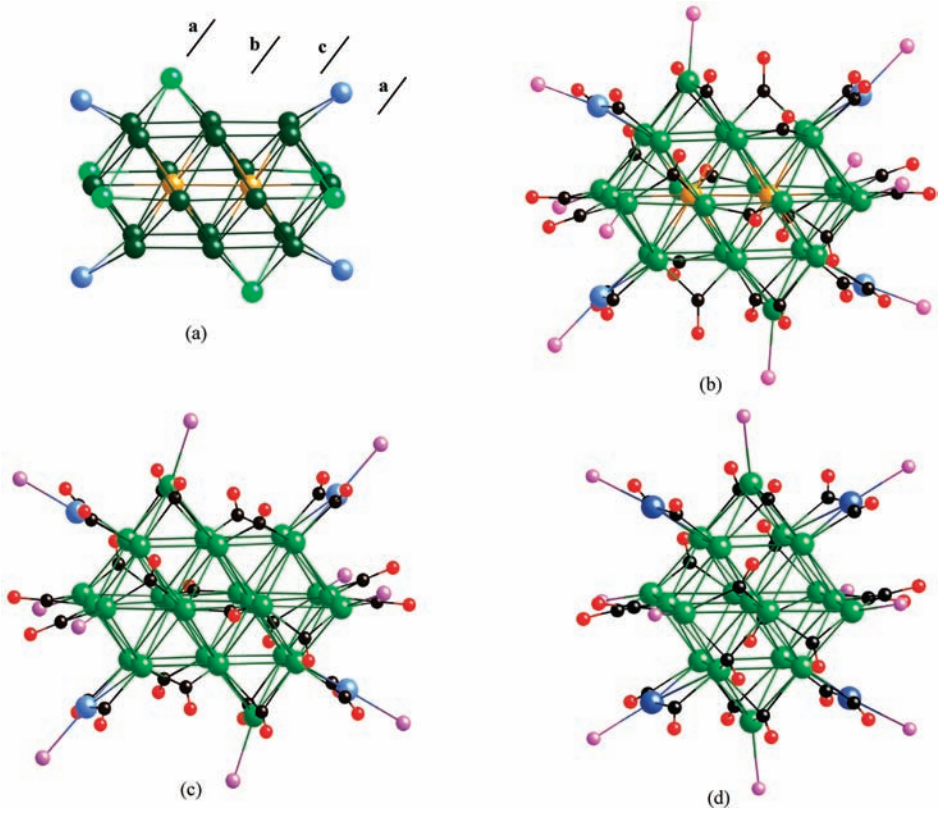

Figure 1. (a) Front view of crystallographic $C_i(\bar{1})$ and *pseudo*-$C_{2h}(2/m)$ Au_2Pd_{28} core geometry of nanosized Au-centered bicuboctahedral-based **1**, considered as a twinned composite of two interpenetrating cuboctahedra. Atom designations are two Au (yellow), 18 Pd(cub) (dark green), two Pd(ap) and four Pd(eq) (light green) that cap six of the eight Pd_4 square faces of the Au_2Pd_{18} bicuboctahedral kernel, and four Pd(exo) (blue). The principal C_2 axis passes through the midpoint of the line connecting the two interior Au atoms, while the perpendicular horizontal σ_h mirror plane contains the two Au and two Pd(cub) atoms in the middle (equatorial) 12-atom $Au_2Pd(cub)_6Pd(eq)_4$ layer, along with the two square-capping Pd(ap) and four wingtip Pd(exo) atoms. The ccp four-layer metal sequence **abca** is shown in bold letters. (b) Front view of **1** with its 10 triethylphosphine P atoms (purple) and 26 bridging CO groups. (c) Analogous front view of corresponding known isostructural Pd-centered bicuboctahedral-based **2**. (d) Front view of known cuboctahedral-based **4**, emphasizing its geometrical resemblance to the front views of (b) **1** and (c) **2**. The bicuboctahedral Pd_{20} kernel of the homopalladium Pd_{30} cluster **2** is considered to be a "twinned" composite of two interpenetrating Pd_{13} cuboctahedra of the Pd_{23} cluster (**4**). Triethyl substituents of P atoms in parts b−d are omitted for clarity.

"open"-square faces. The four triply bridging μ_3-CO ligands connect two opposite triangular Pd(ap)$Pd(cub)_2$ sides formed by the tetracapping of two centrosymmetrically related square $Pd(cub)_4$ faces with the two Pd(cap) atoms. Figure 1b also shows for **1** that the 10 P atoms (without Et substituents) and 26 bridging COs adhere closely to $C_{2h}(2/m)$ symmetry, except for the orientations of the two pairs of μ_2-COs that span opposite edges of the two noncapped "open"-square $Pd(cub)_4$ faces; their observed orientational nonconformity to the *pseudo*-σ_h mirror-plane symmetry in **1** involves one centrosymmetrically related μ_2-CO pair that is highly bent out of the "open" $Pd(cub)_4$ face relative to that of the second moderately bent μ_2-CO pair. In contrast, Figure 1c shows that in the Pd_{30} cluster (**2**) both of these μ_2-CO pairs are moderately bent in accordance with the existence of the *pseudo*-σ_h mirror plane (and resulting close adherence to *pseudo*-C_{2h} symmetry) for all non-H atoms (Et substituents excluded).

Corresponding mean distances between **1** and **2** in Table 1 for the four different Pd−Pd bonding types [viz., those consisting of 40 Pd(cub)−Pd(cub), 16 Pd(cub)−Pd(eq), 8 Pd(cub)−Pd(ap), and 8 CO-linked Pd(cub)−Pd(exo) edges] and for the three different Pd−P bonding types all agree within 0.02 Å. In light of the large 0.1−0.35 Å dispersions (spreads) of individual bonding connectivities for a given Pd−Pd mean distance in these two clusters, the close agreement of corresponding individual distances as well as corresponding bonding mean distances between **1** and **2** emphasizes the remarkable similarity in their bicuboctahedral-based molecular geometries. The observed mean difference of 0.05 Å between the corresponding non-(CO-bridged) Pd(cub)−Pd(exo) distances is expectedly larger because of these four separations of 3.28 Å (av) in **1** and those of 3.33 Å (av) in **2** being essentially nonbonding; on the other hand, the nonbonding Pd(exo)−Pd(ap) distances (of 3.40 and 3.41 Å) in **1** and **2** are nearly identical.

b. Crystallographic Evidence for Strain-Free Interior Pd-by-Au Substitution in ***2***. Despite the large 0.13 Å difference between the bulk metal−metal distance in ccp Au metal (2.884 Å) and that in ccp Pd metal (2.751 Å) at 20 °C,[11] corresponding mean metal−metal bonding distances between **1** and **2** in Table 1 provide self-consistent prime evidence for a strain-free geometrical effect upon the interior Pd-by-Au substitution in **2**: viz., that the radius of each Au atom is only 0.02 Å larger than that of the substituted interior Pd atom in virtually identical ccp sites. This radius difference is given by the 0.02 Å larger radial Au(cent)−Pd(cub) mean distance of 2.86 Å in **1** relative to the radial Pd(cent)−Pd(cub) mean distance of 2.84 Å in **2** for the 22 equivalent M(cent)−Pd(cub) connectivities. Furthermore, this 0.02 Å larger

dx.doi.org/10.1021/ic201923y |*Inorg. Chem.* 2011, 50, 11795–11806

Table 1. Comparative Mean Distances (Å) and Individual Ranges (Å) under *Pseudo*-C_{2h}(2/*m*) Symmetry between the $(\mu_{12}\text{-Au})_2Pd_{28}P_{10}$ Fragment of 1 and Corresponding $(\mu_{12}\text{-Pd})_2Pd_{28}P_{10}$ Fragment of the Known Acetone-Solvated Isostructural 2

distance[a]	*N*[b]	mean [range] in **1**	mean [range] in **2**
M(cent)−M(cent)	1	2.8107(2)	2.773(1)
M(cent)−Pd(cub)	22	2.86 [2.8070(2)−2.9395(3)]	2.84 [2.801(1)−2.877(1)]
Pd(cub)−Pd(cub)	40	2.84 [2.7040(3)−3.0473(3)]	2.83 [2.723(1)−2.965(1)]
Pd(cub)−Pd(eq)	16	2.79 [2.7040(3)−2.8632(3)]	2.81 [2.717(1)−2.908(1)]
Pd(cub)−Pd(ap)	8	2.77 [2.7238(3)−2.8100(3)]	2.77 [2.728(1)−2.810(1)]
Pd(cub)−Pd(exo)[c]	8	2.70 [2.6701(3)−2.7358(3)]	2.71 [2.688(1)−2.732(1)]
Pd(cub)−Pd(exo)[d]	4	3.28 [3.15−3.41]	3.33 [3.22−3.44]
Pd(exo)−Pd(ap)	2	3.40	3.41
Pd(eq)−P	4	2.336 [2.324(1)−2.347(1)]	2.345 [2.337(2)−2.352(2)]
Pd(ap)−P	2	2.329(1)	2.317(3)
Pd(exo)−P	4	2.310 [2.303(1)−2.317(1)]	2.307 [2.306(3)−2.307(3)]

[a] M(cent) designates the two encapsulated centered Au or Pd atoms; Pd(cub) designates the other 18 bicuboctahedral Pd atoms; Pd(eq) designates the four equatorial square-capped Pd atoms; Pd(ap) designates the two apical square-capped Pd atoms; Pd(exo) designates the four exopolyhedral (wingtip) Pd atoms. [b] *N* denotes the total number of individual distances under *pseudo*-C_{2h} symmetry; both **1** and **2** have crystallographically imposed inversion centers. [c] Pd(cub)−Pd(exo) distances edge-bridged by COs. [d] Pd(cub)−Pd(exo) distances devoid of bridging CO ligation.

gold radius is consistent with the Au−Au distance of 2.811(1) Å between the two interior Au(cent) atoms in **1** being 0.04 Å larger than the Pd(cent)−Pd(cent) distance of 2.773(1) Å in **2**. The fact that the Au−Au distance is larger (instead of smaller) also signifies the *absence* of a *localized* Au−Au σ bond (vide infra).

The 0.02 Å larger Au(cent)−Pd(cub) mean distance of 2.86 Å in **1** than in nonsubstituted **2** is likewise in agreement with the corresponding Au(cent)−Pd(cub) mean distances of 2.87 Å in $Au_2Pd_{21}(CO)_{20}(PAlk_3)_{10}$ [Alk = Et (**3**), Me] and 2.86 Å in $[AuPd_{22}(CO)_{20}(PPh_3)_4(PMe_3)_6]^-$ that are similarly ca. 0.02 Å larger than the corresponding Pd(cent)−Pd(cub) mean distance of 2.84 Å in the nonsubstituted cuboctahedral-based $Pd_{23}(CO)_{20}(PEt_3)_{10}$ (**4**) analogue.

*c. Geometric Relationship of the Interpenetrating Bicuboctahedral Au_2Pd_{28} **1** with Corresponding Cuboctahedral Au_2Pd_{21} **3** and Structurally Related $[AuPd_{22}]^-$ Monoanion.* The CO/PR_3-ligated geometry of the Au_2Pd_{28} **1** represents an unprecedented example conceptually involving Pd-by-Au substitution at *exclusively interior* sites of the isostructural Pd_{30} **2** with an otherwise nearly indistinguishable entire geometry from that of the homopalladium **2**. In contrast, conceptual generation of the known $Au_2Pd_{21}(CO)_{20}(PEt_3)_{10}$ (**3**) from the isostructural triethylphosphine-ligated **4** (Figure 1d) involves Pd-by-Au replacements at the Pd-centered atom and one of the Pd_4-capped surface Pd atoms, thereby lowering the *pseudo* metal-core symmetry from D_{2h} to C_{2v}.[6a] On the other hand, an exchange of only the central encapsulated Pd atom by Au (coupled with an added valence electron) in the D_{2h} Pd_{23} metal ore of **4** is exemplified by the $[AuPd_{22}(CO)_{20}(PPh_3)_4(PMe_3)_6]^-$ monoanion; however, its $AuPd_{22}$ core eometry possesses *pseudo*-T_d symmetry because of the resulting "migration" of two of the four exopolyhedral Pd atoms from their centrosymmetric coplanar-disposed orientations in **4** to nonadjacent tetrahedrally disposed ν_2 triangular Pd_6 planes of the centered ν_2 $AuPd_{18}$ octahedron;[6a] it is presumed that this metal-core rearrangement of the exopolyhedral Pd atoms may be induced by the four relatively bulky PPh_3 ligands attached to the four exopolyhedral Pd atoms.

Theoretical Analysis of Natural Atomic Charge Distributions in Au_2Pd_{28} (1-H) and Pd_{30} (2-H) Models of 1 and 2 and in Their Hypothetical $[1\text{-H}]^{2+}$ and $[2\text{-H}]^{2-}$ Analogues. *a. Methodology.* DFT calculations were performed by use of the *Gaussian 09* computational package.[12] The hybrid gradient-corrected (generalized gradient approximation, GGA) DFT functional B3PW91, which combines the Becke three-fitted parametrization scheme[13] with a nonlocal PW91 correlation treatment,[14] was our method of choice. The scalar-relativistic effective core potential (ECP) basis set (LANL2DZ) of Hay and Wadt[15] was employed for Pd, Au, and P atoms. It includes the LANL2 ECP treatment of core electrons with an explicit treatment of the outermost core and valence electrons. For a more flexible treatment of ligand atoms, one polarization d function was added to each P atom.[16] The Pople 6-31G* all-electron basis set[17] was used for C, O, and H atoms. Natural population analysis (NPA) was performed by use of the *NBO 5.0* stand-alone software package.[18] For computational modeling of **1** and **2**, model clusters $Au_2Pd_{28}(CO)_{26}(PH_3)_{10}$ (**1-H**) and $Pd_{30}(CO)_{26}(PH_3)_{10}$ (**2-H**), together with hypothetical $[Au_2Pd_{28}(\mathbf{1\text{-H}})]^{2+}$ and $[Pd_{30}(\mathbf{2\text{-H}})]^{2-}$ analogues, were utilized, for which all PEt_3 phosphine ligands were replaced by computationally more tractable PH_3 ones,[6h] with each P−H bond and each Pd−P−H angle fixed at 1.4 Å and 116°, respectively. Because it was crystallographically established that the entire geometries of both **1** and **2** are essentially isostructural and in order to avoid the computationally prohibitive geometry optimizations of these model clusters, the **1-H** model was generated from the **2-H** model by replacement of the two interior Pd atoms with Au atoms, together with consecutive elongation of the Au−Au connectivity by 0.04 Å (in accordance with the crystallographic findings).

b. Resulting Theoretical Implications. Table 2 gives the resulting charges obtained from NPA carried out on the isostructural **1-H** and **2-H** model clusters of **1** and **2** containing cores comprised of two interior metal atoms and 28 Pd surface atoms that are ligated by 26 CO and 10 PH_3 groups (i.e., with phosphine Et substituents replaced by H atoms). For comparison, similar calculations were also performed on the hypothetical $[Au_2Pd_{28}(\mathbf{1\text{-H}})]^{2+}$ dication, which is electronically equivalent to $Pd_{30}(\mathbf{2\text{-H}})$, and on the hypothetical $[Pd_{30}(\mathbf{2\text{-H}})]^{2-}$ dianion, which is electronically equivalent to $Au_2Pd_{28}(\mathbf{1\text{-H}})$.

For the above four clusters, this NPA shows that the electron density distributions between each of the two types of CO and PH_3 ligands, and the metal cores are remarkably similar. Table 2 discloses highly positively charged Pd_{28} surfaces (range +3.43e to +3.84e) relative to both negatively charged interior metal atoms. These are indicative of a partially oxidized metal surface that

dx.doi.org/10.1021/ic201923y |*Inorg. Chem.* 2011, 50, 11795–11806

Table 2. Average Natural Atomic Charges on Metal Atoms and Ligands for Isostructural Model Clusters 2-H and 1-H and Hypothetical $[1\text{-H}]^{2+}$ and $[2\text{-H}]^{2-}$

	$Pd_{30}(\mathbf{2\text{-H}})^a$		$Au_2Pd_{28}(\mathbf{1\text{-H}})^a$		$[Au_2Pd_{28}(\mathbf{1\text{-H}})]^{2+a}$		$[Pd_{30}(\mathbf{2\text{-H}})]^{2-a}$	
charge[b]	total Q	Q per unit[c]	total Q	Q per unit[c]	total Q	Q per unit[c]	total Q	Q per unit[c]
q(core)	+2.874	+0.096	+3.061	+0.102	+3.339	+0.111	+2.595	+0.087
$q(M_{interior})$	−0.964	−0.482	−0.369	−0.185	−0.317	−0.158	−1.146	−0.573
$q(Pd_{surface})$	+3.838	+0.137	+3.430	+0.123	+3.656	+0.131	+3.741	+0.134
q(CO)	−5.045	−0.194	−5.166	−0.199	−4.092	−0.157	−6.143	−0.236
$q(PH_3)$	+2.171	+0.217	+2.105	+0.210	+2.753	+0.275	+1.547	+0.155

[a] Each metal core consists of 2 $M_{interior}$ and 28 $Pd_{surface}$ atoms ligated by 26 CO and 10 PH_3 groups. [b] All charges are in electrons. [c] "Q per unit" denotes either charge per metal atom or charge per ligand.

results from the negatively charged 26 CO ligands (range −4.09e to −6.14e in total) due to dominant (CO) back-bonding of the bridging carbonyl ligands. Close to 40% of the electron density accumulated on the COs in Au_2Pd_{28}(**1-H**) (−5.17e) and Pd_{30}(**2-H**) (−5.05e) originates from the σ-donor PH_3 ligands, as evidenced by their similar acquired positive charges of +2.11e and +2.17e in Au_2Pd_{28}(**1-H**) and Pd_{30}(**2-H**), respectively. Much different positive charges are expectedly observed for the PH_3 ligands in the hypothetical $[Au_2Pd_{28}(\mathbf{1\text{-H}})]^{2+}$ dication (+2.75e) and $[Pd_{30}(\mathbf{2\text{-H}})]^{2-}$ dianion (+1.55e) in accordance with the overall cluster charge.

In contrast to the 28 Pd surface atoms, NPA reveals the existence of negative charges on both interior metal atoms in all four model clusters. This buildup of electron density on the two interior atoms likely arises from the energy lowering of core $(n-1)$d and valence ns atomic orbitals of Pd or Au due to more efficient electron delocalization from these interior atoms. Of particular importance is that Table 2 provides a comparative analysis of the charge rearrangements upon the formal replacement of the two $Pd_{interior}$ atoms in Pd_{30}(**2-H**) by two Au atoms to give Au_2Pd_{28}(**1-H**). In this case, the total positive charge of +2.87e on the entire Pd_{30}(**2-H**) core increases to +3.06e for the entire Au_2Pd_{28}(**1-H**) core. However, the unexpected observation in Table 2 that the two $Pd_{interior}$ atoms in **2-H** are more negatively charged by 0.60e than the corresponding two Au atoms in **1-H** is completely contrary to the general expectation in that neutral Au atoms are considerably more electronegative[19,20] than neutral Pd atoms. We propose that this reversal in the expected charge-density distribution is a consequence of the Au atoms in **1-H** being much more cationic than the two interior Pd atoms in **2-H** because of extensive delocalization of each 6s Au electron toward a formal closed-shell valence ground-state description of a Au^+ $6s^0 5d^{10}$ configuration. In particular, we believe that the significant decrease in the negative charge of the interior Au atoms in **1-H** compared to that of the interior Pd atoms in **2-H** is likely caused by two competing processes. On the one hand, the more electronegative Au should acquire an even more negative charge than Pd. The effect of a *higher* electronegativity of interior metal atoms on their partial charge can readily be shown by replacement of the two interior Pd atoms in **2-H** with Pt, which has a higher electronegativity nearer to that of Au. Indeed, the partial charge on each interior Pt atom in the hypothetical Pt_2Pd_{28} model analogue of Pd_{30}(**2-H**) is significantly more negative (−0.68e) than that on each interior Pd atom (−0.48e). On the other hand, the substitution of two interior Pd atoms in **2-H** with Au to give **1-H** gives rise to one extra valence electron for each Au. The participation of two Au 6s electrons in delocalized cluster bonding would cause depletion of the electron density on the interior Au atoms and would thereby make the partial charge on Au more positive. The combination of these two effects is likely responsible for the much smaller but still negative charge of −0.19e on each Au atom in **1-H**. Furthermore, the total positive charge of +3.43e for the Pd_{28} surface atoms in Au_2Pd_{28}(**1-H**) being markedly less positive (more negative) than that of +3.84e in Pd_{30}(**2-H**) along with the corresponding total charges for the 26 CO and 10 PH_3 ligands being slightly more negative in **1-H** relative to **2-H** by −0.12e and −0.07e, respectively, suggest that delocalization of the two 6s Au valence electrons extends over the entire cluster of **1**.

The results of the Wiberg bond index (WBI) calculations[21] are in agreement with this premise. The calculated WBI value for the Au−Au bond in **1-H** is only 0.055, which is slightly greater than the WBI value of 0.032 for the average Pd−Au bond of 2.86 Å within the same cluster. In sharp contrast, the WBI value obtained from analogous DFT calculations for the bare, neutral Au_2 dimer is 1.01; this Au−Au bond order that signifies a single bond is attributed to the two Au 6s electrons forming a "localized" electron-pair interaction. Further support for this strong "covalent" bonding interaction in the Au_2 dimer is given by the short spectroscopically measured Au−Au distance of 2.472 Å for Au_2 in the gas phase.[22] It is apparent that any type of ligation or additional coordination to other metal atoms would increase delocalization of the two "localized" Au 6s electrons in the Au_2 dimer and thereby would elongate the corresponding Au−Au distance.[23] Ultimately, an interaction between two $6s^0 5d^{10}$ Au^+ cations (with no 6s electrons), which has been denoted as a so-called aurophilic attraction,[24,25] would give rise to a Au−Au separation of ∼3.0 Å, corresponding to WBI being approximately zero. Hence, because of the presumed cationic nature of the two Au atoms in **1**, one might expect its Au−Au separation to be even larger than the crystallographically observed distance of 2.811(1) Å. However, the *matrix effect* involving each 12-coordinated ccp Au atom in **1** being "embedded" within the Pd_{28} framework, which, in turn, is stabilized by the bridging carbonyl and phosphine ligands, provides an electronic/structural balance. As indicated from the crystallographic comparison between the metal cores in the isostructural Au_2Pd_{28} **1** and Pd_{30} **2**, an *ideal site-occupancy fit* exists between the two interior Au atoms in **1** and corresponding interior Pd atoms in **2**, in accordance with their closely related molecular parameters.

Table 2 also shows that "double oxidation" of Au_2Pd_{28}(**1-H**) to its $(\mathbf{1\text{-H}})^{2+}$ dication results in the entire Au_2Pd_{28} core becoming less negative by only 0.28e, with the partial negative charge on the two Au atoms remaining essentially unaltered (with only a +0.05e increase). Similar behavior is observed upon the

dx.doi.org/10.1021/ic201923y |*Inorg. Chem.* 2011, 50, 11795–11806

two-electron reduction of Pd_{30}(**2-H**) to its $[$**2-H**$]^{2-}$ dianion; the entire Pd_{30} core becomes more negative by only 0.28e, with the partial negative charge on the two interior Pd atoms increasing by 0.18e. Thus, either a "double oxidation" of Au_2Pd_{28}(**1-H**) or a "double reduction" of Pd_{30}(**2-H**) primarily involves large charge variations on the 26 COs (by 1.1e) and on the 10 PH_3 ligands (by 0.6e). These large ligand charge variations point to the crucial influence of the particular PR_3/CO ligation as an "electron buffer", which upon electron addition/removal supplies the required amount of electron density to stabilize the metal core.

Synthesis and Spectroscopic Characterization of 1. *a. Two-Step Synthetic Procedure.* The Au_2Pd_{28} cluster **1** was initially isolated from the reaction of $Pd_{10}(CO)_{12}(PEt_3)_6$ (**5**)[26] with $Au(SMe_2)Cl$.[27] This pathway (eq 1) combined two sets of reaction conditions; the first step (a), which involves reaction in an acetone/acetic acid solvent mixture at 50 °C under an inert (N_2) atmosphere, was previously utilized to generate the *cuboctahedral-based* **4**.[6e] The second step (b) consists of a prolonged reaction of the tetrahydrofuran (THF) extract (obtained from the resulting black precipitate, BP, in step (a) *with CO*.

$$\underset{(\mathbf{5})}{Pd_{10}(CO)_{12}(PEt_3)_6} + Au(SMe_2)Cl \xrightarrow[\text{(b) rt, THF, CO}]{\text{(a) 50 °C, } Me_2CO/HOAc, N_2} \underset{(\mathbf{1})}{Au_2Pd_{28}(CO)_{26}(PEt_3)_{10}} \quad (1)$$

The *only difference* between the first step (a) from the known conversion of **5** to the $Pd_{23}P_{10}$ cluster **4**[6e] is the additional involvement of $Au(SMe_2)Cl$, which converts eq 1 into a redox reaction. Concerning step b, it should be noted that preliminary saturation of solutions by CO, although only for a short time (1−2 h), was always necessary for generation of the isostructural homopalladium **2**.[6g,9] Of prime importance is that the use of N_2 instead of CO in the second step (b) *prevents* the formation of **1**. Thus, an IR spectrum (Nujol) of crystalline material isolated from this latter reaction (under N_2) displayed a strong broad bridging carbonyl band at 1882 cm^{-1} that is typical of *particularly large* Pd_n carbonyl/phosphine clusters ($n > 60$). Unfortunately, this crystalline material did not provide suitable single crystals for an X-ray diffraction study.

Other coproducts originating from a detailed experimental examination of the reaction conditions of this two-step procedure (see the Experimental Section and Figure 1s in the Supporting Information) were identified from single-crystal X-ray diffraction and/or IR and $^{31}P\{^1H\}$ NMR measurements; these included **4**,[6e] **3**,[6a] $Pd_{16}(CO)_{13}(PEt_3)_9$,[6j] $Pd_{34}(CO)_{24}(PEt_3)_{12}$,[6k,l] $Pd(PEt_3)_2Cl_2$,[28,29] and the CO-regenerated precursor **5**.[26,30,31] The types and yields of the cluster coproducts were found to depend crucially upon whether the reactions were carried out under a CO or N_2 atmosphere. Analyses of their compositions provided important insights into the two-step procedure and led to the finding of a second *direct* way to produce **1** via the CO-induced reaction of cuboctahedral-based **3** with **4**.

*b. One-Step Synthesis from **3** and **4** under a CO Atmosphere and Resulting Implications.* A second pathway to **1** is via the direct nonredox reaction in THF of the isostructural **3** and **4** under a CO atmosphere (eq 2).

$$\underset{(\mathbf{3})}{Au_2Pd_{21}(CO)_{20}(PEt_3)_{10}} + \underset{(\mathbf{4})}{Pd_{23}(CO)_{20}(PEt_3)_{10}} \xrightarrow[\text{THF, rt}]{CO} \underset{(\mathbf{1})}{Au_2Pd_{28}(CO)_{26}(PEt_3)_{10}} \quad (2)$$

Notably, the reaction of **3** and **4** under a N_2 atmosphere did not afford **1**, similar to the effect of CO-by-N_2 substitution in the second step in the two-step procedure. Only crystals of the initial coreactant **3** were isolated from the resulting solution under N_2 and identified from X-ray diffraction measurements; in addition, a $^{31}P\{^1H\}$ NMR spectrum of this solution under N_2 exhibited strong signals [δ_1 = 14.0 ppm (s), δ_2 = 9.7 ppm (s), with a 1:1 intensity ratio] characteristic of the other known Pd_{23} cluster, $Pd_{23}(CO)_{20}(PEt_3)_8$ (**7**)[6o−q] as the dominant product instead of **4**, which was not detected. The presence of **7**, which possesses the same Pd_{23} nuclearity and the same number of CO ligands but two fewer PEt_3 ligands than **4**, is *not* surprising. This other $Pd_{23}P_8$ cluster (**7**), which has a highly dissimilar metal-core architecture comprised of an extensively deformed centered hexacapped cubic Pd_{15} kernel (of *pseudo-D_{2d}* symmetry) with eight capping Pd atoms, was previously shown to arise via conversion of **4** under N_2 (eq 3), either induced by O_2 (air)[6q] or moderately elevated temperature or electrochemically[6e]

$$\underset{(\mathbf{4})}{Pd_{23}(CO)_{20}(PEt_3)_{10}} \xrightarrow{-2[PEt_3]} \underset{(\mathbf{7})}{Pd_{23}(CO)_{20}(PEt_3)_8} \quad (3)$$

The facile lability of these two PEt_3/CO-ligated Pd_{23} clusters **4** and **7** in undergoing rapid PEt_3-induced reversible interconversions into each other in spite of their completely different Pd_{23} core geometries is due to a ligation difference of only two PEt_3 groups. This chemically induced reversible geometrical interconversion in solution was clearly demonstrated from a $^{31}P\{^1H\}$ NMR monitored investigation[6q] and was readily ascribed to markedly weaker M−M and M−CO bonding connectivities in palladium carbonyl clusters compared to those in nickel and platinum carbonyl clusters.[6q,r,8]

Hence, the *CO-induced* formation of **1** from **3** and **4** in eq 2 versus the isolation of the intact Au_2Pd_{21} precursor (**3**) *under N_2* in an otherwise analogous procedure provides convincing evidence concerning the key synthetic role of CO being necessary for the preparation of **1**. Moreover, the relative stability of the Au_2Pd_{21} cluster (**3**) under CO versus the known fragmentation of the $Pd_{23}P_{10}$ cluster (**4**) under CO led us to conclude that reactive coordinatively unsaturated fragments (CUFs) of **4**, generated under CO, initiate the formation of **1**. Control reactions of $Pd_{23}P_{10}$ **4** and Au_2Pd_{21} **3** in THF solutions with CO performed at 50 °C showed the complete disappearance of $^{31}P\{^1H\}$ NMR signals of **4** after 30 min, whereas approximately 60% of those of **3** were still intact after a 2 h reaction.

In general, the facile lability of palladium carbonyl/phosphine clusters to undergo metal-framework transformations via their simple exposure either under conventionally inert N_2 or Ar atmospheres (as shown here and earlier[6e,8]), vacuum,[6s] or CO[6s,8] is responsible for a variety of observed products (see Figure 1s in the Supporting Information). Complete rearrangement of the entire metal core may occur and commonly may concomitantly take place along with fragmentation/growth processes.[6q,r,8] Even though such transformations are thermodynamically driven, the observed $Pd_n(CO)_x(PR_3)_y$ products can generally be kinetically controlled.[8]

Proposed Chemically Induced Assembly of the Au_2Pd_{28} Core Geometry of 1 from the Au_2Pd_{21} Core Geometry of 3 via Reactions with Coordinatively Unsaturated CO/PEt_3-Ligated Species. Under a *renewable/unrestricted supply of CO* and duration of reactions for several days, solutions of homopalladium Pd_{16}, $Pd_{23}P_{10}$, and Pd_{38} clusters gave two ultimate kinetically/thermodynamically stable products, **5** and Pd black.[6s]

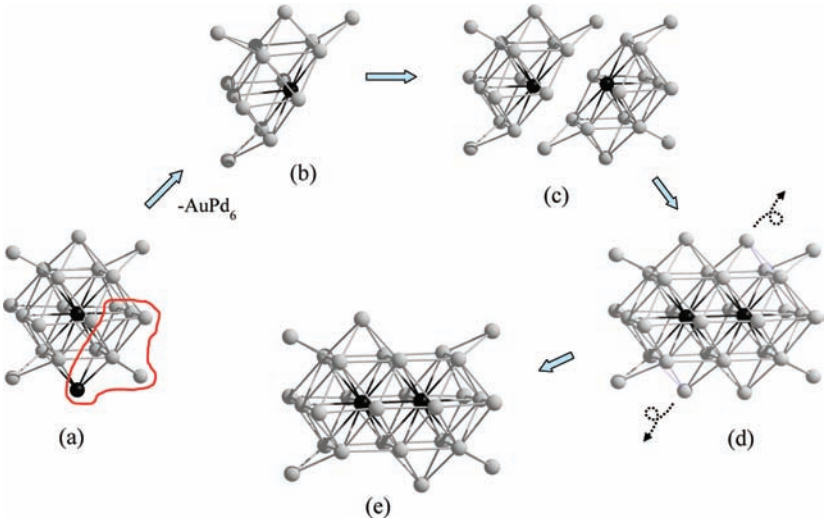

Figure 2. Structural diagram of a possible intercluster pathway in the formation of the Au_2Pd_{28} core geometry in **1** from the CO-stable Au_2Pd_{21} precursor **3** by chemical activation reactions with CUFs of homopalladium CO/PR_3-ligated species generated from CO-induced fragmentation of either structurally similar **4** or structurally dissimilar **6**. (a → b) Elimination of the outer seven-atom Pd-capped ν_2 $AuPd_5$ triangular layer of the three-layer Au_2Pd_{21} **3** via reactions with CUFs. (b → c and d) Free condensation of two resulting two-layer $AuPd_{15}$ fragments into a centrosymmetric four-layer ccp Au_2Pd_{30} dimer with an encapsulated Au−Au moiety. (d → e) Elimination of two centrosymmetrically related square-capped Pd atoms giving rise to the formation of a Au_2Pd_{28} core of **1**.

Evidently, both products resulted from fragmentation/condensation processes involving CUFs, where Pd black is a simplified designation for giant CO/PR_3-ligated Pd_n particles with $n \gg 100$. Moreover, **5**, *which is stable only under CO*, can be generated by the treatment of freshly prepared Pd black with CO and PEt_3.[6s] These observations led to our hypothesis that the direct synthesis of Au_2Pd_{28} **1** from the reaction under CO of the CO-stable Au_2Pd_{21} **3** with CO-unstable Pd_{23} **4** actually involves the reaction of **3** with CUFs generated from a prior CO-induced fragmentation of **4**. Consequently, we then performed an analogous reaction of Au_2Pd_{21} **3** with CO-unstable $Pd_{38}(CO)_{28}(PEt_3)_{12}$ (**6**),[6l,t] which geometrically is completely unlike **4**. This latter reaction also afforded the Au_2Pd_{28} **1** in similar yield and as the only crystalline product. We concluded that the assembly of **1** from **3** does not necessitate a second reagent with a geometry closely related to that of **1** or **3** (viz., **4**) but instead only one with a similar reactivity toward CO that gives rise to CUFs.

These fragmentation reactions of CO-unstable **4** or **6**, which are presumed to give rise to CUFs, could include only carbonyl species such as $Pd_n(CO)_x$ (e.g., $n = 1, 2$; $x = 1-4$) as well as CO/PR_3 species such as $Pd_n(CO)_x(PEt_3)_y$ (e.g., $n = 1, 2$; $x = 1$; $y = 1$). Similar CUFs were proposed earlier as explanations for well-established growth reactions (viz., Pd_1 Pd_3, Pd_3 Pd_4, and Pd_4 Pd_{10}) that occur in the family of $Pd_n(CO)_x(PR_3)_y$ clusters under a CO atmosphere.[31b] The formation of CUFs was also postulated to arise from the reaction of $Pd(dba)_2$ with CO (where dba denotes dibenzylideneacetone);[32] moreover, highly reactive binary palladium carbonyl fragments, $Pd(CO)_x$ (with $x = 1-4$), were observed in inert matrices at cryogenic temperatures.[33] It should be emphasized that suggested compositions of fragmentation products are simplified in that they represent only the smallest mono- and binuclear building blocks. Obviously, three, four, and, likely, higher nuclear species can be generated and participate in further condensations.

The CUF-induced cluster assembly of the Au_2Pd_{28} core in **1** may involve a complicated *intracluster* rearrangement of the two separated Au atoms in the Au_2Pd_{21} **3** into the internally connected Au atoms in **1** along with concomitant CUF face condensations. Alternatively, a possible greatly simplified *intercluster*-assembly pathway is depicted in Figure 2, whereby the two adjacent Au atoms in **1** originate from two separate Au_2Pd_{21} clusters (**3**). This scheme assumes elimination of the seven-atom Pd-capped ν_2 $AuPd_5$ triangular layer of the **abc** ccp three-layer Au_2Pd_{21} **3** via reactions with CUFs followed by a face condensation of two resulting two-layer $AuPd_{15}$ fragments into a centrosymmetric four-layer **abca** ccp Au_2Pd_{30} dimer; the Au_2Pd_{28} **1** is then produced by the elimination of two centrosymmetrically related square-capped Pd atoms. Noteworthy is the discovery of an analogous cocrystallized 7% impurity in two virtually identical (completely refined) structural determinations of **1** that additionally consists of two designated Pd atoms occupying these same two centrosymmetrically related square-capped metal sites (vide infra).

Spectroscopic Characterization of ***1***. Solid-state (Nujol) IR spectra of **1** obtained from the above-mentioned procedures exhibited three strong bands at 1911, 1886, and 1860 cm^{-1} along with weak or shoulder bands at 1842−1840, 1821, 1806, and 1779−1776 cm^{-1} in accordance with the doubly and triply bridging carbonyl coordination modes found in both virtually identical crystal structures of **1** (vide infra). The detection of a weak band at 2028−2022 cm^{-1} characteristic of a terminal CO may be associated with the same above-mentioned minor superimposed cocrystallized impurity in both crystal structures containing two additional centrosymmetrically refined Pd atoms, of which each is proposed from stereochemical considerations to be coordinated to a terminal carbonyl ligand (vide infra).

Because crystals of **1** were insoluble in nonchlorinated solvents, a $^{31}P\{^1H\}$ NMR spectrum was obtained in a CD_2Cl_2 solution; because its solubility was still poor, several hundred scans were necessary in order to obtain a satisfactory spectrum. It should be noted that for CO/PR_3-ligated palladium clusters chlorinated solvents are generally not the best choice due to the

dx.doi.org/10.1021/ic201923y |*Inorg. Chem.* 2011, 50, 11795–11806

possible oxidative addition reactions. Nevertheless, the $^{31}P\{^1H\}$ NMR spectrum of **1** revealed four prime broad signals at δ_1 = 14.8 ppm, δ_2 = 8.4 ppm, δ_3 = 6.8 ppm, and δ_4 = 3.8 ppm with intensity ratios of δ_1:(δ_2 + δ_3):δ_4 = 1:3:1 (the two overlapping δ_2 and δ_3 signals gave an estimated intensity ratio of 1:2). The number of these signals and their approximate relative intensities are consistent with the *pseudo*-C_{2h} molecular geometry of **1**, for which the 10 PEt_3 ligands are distributed among four distinctly different Pd-coordinated P atoms as follows: four P atoms each attached to one of two types of four (exopolyhedral) wingtipped Pd atoms, two P atoms each attached to one of two square-capped apical Pd atoms, and four P atoms each attached to one of four symmetry-equivalent square-capped equatorial Pd atoms. No $^{31}P\{^1H\}$ NMR spectrum of **2** was available because of its low yield and relative insolubility.[9]

Electron-Counting Analysis of ***1***. The observed electron count of 374 electrons [(2 × 11)Au + (28 × 10)Pd + (26 × 2)CO + (10 × 2)PEt_3] for **1** is in accordance with the Ciani/Sironi model,[34] which defines the number of cluster valence molecular orbitals as $6N_M + X$ (where N_M denotes the total number of metal atoms, and an average value of 7 is normally used for X). Application of the Mingos model[35] for **1** gives either (a) 378 electrons based upon the geometry of **1** being considered as an edge condensation of an Au_2Pd_{24} fragment with four wingtipped metal triangles [viz., 12 × 24 (surface) + 34 (two encapsulated) + 4 × 14 (wingtip)] or (b) 370 electrons based upon the calculated Mingos model[35] applied to Au_2Pd_{28} being given by $\Delta_i + 12n_s$, where n_s is the number of surface atoms (viz., 28) and Δ_i is the number of electrons for the central M_2 fragment (viz., 34). The latter electron count of 370 electrons is also obtained from the Teo/Zhang model,[36] for which $N = 2[6G + K]$, where G is the total number of metal atoms (viz., 30) and K = 5 for an encapsulated M_2 dimer centered at a hole. The fact that the calculated electron counts from these theoretical models do not necessarily correspond to the observed number of cluster valence electrons is not surprising, especially in light of the ability of CO/PR_3-ligated Pd_n clusters to possess a variable number of CO ligands on otherwise unchanged metal polyhedra, as exemplified by $Pd_{23}(CO)_x(PEt_3)_{10}$ clusters (with x = 20−22).[7]

CONCLUSIONS

This synthesis of **1** illustrates an important breakthrough in the formation of new nanosized heterometallic palladium clusters by utilization of CO-induced fragmentation of CO-unstable homopalladium CO/PR_3-ligated clusters (viz., Pd_{23} **4** or Pd_{38} **6**) to transform a CO-stable Au−Pd cluster (viz., Au_2Pd_{21} **3**) into one of higher nuclearity (viz., into Au_2Pd_{28} **1**).

The entire molecular geometry of **1** may be formally derived by replacement of the *interior* $(\mu_{12}\text{-Pd})_2$ moiety in **2** with the nonisovalent *interior* $(\mu_{12}\text{-Au})_2$ moiety in an otherwise essentially unaltered palladium/ligand geometry. In contrast to the synthesis of **2**, which requires relatively short-time CO assistance at the initial stage of the reaction followed by crystallization under N_2, the preparation of **1** occurs exclusively under a CO atmosphere. Such stability toward CO was also observed for Au_2Pd_{21} **3** versus either the isostructurally CO-unstable Pd_{23} **4** or the structurally dissimilar CO-unstable Pd_{38} **6**. The virtually *ideal geometrical site-occupancy fit* between **1** and **2** is demonstrated from a comparison of the corresponding mean metal−metal bonding distances (Table 1) between **1** and **2**: the radius of each interior Au in **1** is only 0.02 Å larger than that of the two substituted 12-coordinated Pd atoms in presumed identical interior ccp sites, and the corresponding observed increase in the Au−Au distance is 0.04 Å. These small self-consistent crystallographic changes provide the experimental basis of our hypothesis for delocalization of the two Au 6s valence electrons (instead of a "localized" electron-pair Au−Au interaction).

Gradient-corrected, pseudo-scalar-relativistic DFT calculations were carried out for the virtually identical entire geometries of the zerovalent Au_2Pd_{28} **1-H** and Pd_{30} **2-H** model clusters along with hypothetical $[\mathbf{1\text{-}H}]^{2+}$ and $[\mathbf{2\text{-}H}]^{2-}$ analogues (without computationally prohibitive geometry optimizations and with all phosphine Et substituents in **1** and **2** being replaced by H ones). NPA of these four model systems revealed similar highly positively charged Pd_{28} surfaces relative to both negatively charged interior metal atoms, which is attributed to dominant CO back-bonding producing a partially oxidized metal surface. Particularly noteworthy is that the total positive surface charge for the 28 Pd surface atoms (range +3.4e to +3.8e) in the four model clusters was relatively unaffected (within 12%) either by the formal interior Pd-by-Au replacement or by the hypothetical two-electron redox changes of **1-H** and **2-H** to their 2+ and 2− ions, respectively. The fact that each interior Pd atom in **2-H** is more negatively charged by 0.30e than each Au atom in **1-H** suggests that the two Au atoms in **1** are more *cationic* than the two interior Pd atoms in **2**; this counterintuitive charge difference (based upon neutral Au being much more electronegative than neutral Pd) is consistent with our premise, initially formulated from the crystallographic evidence, involving substantial delocalization of the two Au 6s valence electrons toward a formal closed-shell valence ground-state description of Au^+ $6s^05d^{10}$. This conclusion is in agreement with WBI calculations that predict a Au−Au bond order in **1-H** of only 0.055, which is slightly greater than the WBI value of 0.032 calculated for the average Pd−Au distance of 2.86 Å. In sharp contrast, from analogous DFT calculations on the bare, neutral Au_2 dimer, the calculated WBI value of 1.01 signifies a Au−Au single bond (corresponding to a "localized" electron-pair interaction); this value is completely consistent with a much shorter spectroscopically measured Au−Au distance of 2.472 Å for the Au_2 dimer in the gas state. Similar charge-transfer behavior was revealed upon either a two-electron oxidation of Au_2Pd_{28}(**1-H**) to its $[\mathbf{1\text{-}H}]^{2+}$ or a two-electron reduction of Pd_{30}(**2-H**) to its $[\mathbf{2\text{-}H}]^{2-}$; in sharp contrast to small analogous charge variations (within ∼10%) that occur within their metal cores, large charge variations were observed for the CO and PH_3 ligands. These DFT calculations thereby emphasize the crucial role of PR_3/CO ligation in these nanosized homopalladium/heterometallic palladium clusters as "electron buffers" that furnish the necessary electron density required for cluster stabilization. These experimental/theoretical implications give new insight concerning the possible incorporation of Au into the mixed ccp/hcp frameworks of other nanosized zerovalent palladium clusters, such as $Pd_{52}(CO)_{36}(PEt_3)_{14}$, $Pd_{54}(CO)_{40}(PEt_3)_{14}$, and $Pd_{66}(CO)_{45}(PEt_3)_{16}$.[8] This research especially emphasizes the importance of CO-induced reactions as a preparative pathway to new Au−Pd clusters via the fragmentation of large homopalladium carbonyl/phosphine clusters under a CO atmosphere.

Of major significance to nanoscience/nanotechnology is that isolation of **1** under CO has been established in well-defined CO/PR_3-ligated digold-substituted Au_2Pd_{n-2} clusters [viz., n = 30 (**1**) and 23 (**3**)] and that their relative stabilizations from decomposition processes under CO are *not* markedly influenced by whether the two Au atoms are adjacent (as in **1**) or separated (as in **3**). This important finding is directly linked to the recent

literature report[37] on (metal−organic framework, MOF)-immobilized Au−Pd nanoparticle composites being highly active catalysts for the complete conversion of formic acid into high-quality hydrogen (and CO_2) at a convenient temperature for chemical hydrogen storage; it was stated that these "Au−Pd nanoparticle catalysts with strong bimetallic synergistic effects have a much higher catalytic activity and a higher tolerance with respect to CO poisoning than monometallic Au and Pd counterparts". This report[37] also clearly demonstrated that the presence of Au likewise prevents CO poisoning: whereas the MOF-immobilized catalysts were observed under CO to still maintain 100% activity and selectivity for dehydrogenation of formic acid, the corresponding Pd counterpart material became deactivated early in the decomposition of formic acid because of CO poisoning.

EXPERIMENTAL SECTION

Materials and Techniques. Reactions were carried out via standard Schlenk techniques on a preparative vacuum line under a controlled atmosphere. All solvents were deoxygenated prior to use by purging with an N_2 flow for at least 20 min at room temperature. $Pd_{10}(CO)_{12}(PEt_3)_6$ (**5**) was prepared as described for $Pd_{10}(CO)_{12}(PBu^n_3)_6$[6m] and purified by recrystallization from C_6H_6/heptane. $Au_2Pd_{21}(CO)_{20}(PEt_3)_{10}$ (**3**), $Pd_{23}(CO)_{20}(PEt_3)_{10}$ (**4**), and $Pd_{38}(CO)_{28}(PEt_3)_{12}$ (**6**) were prepared in accordance with literature procedures.[6a,e,l] Other chemicals were purchased and used without additional purification. Ambient-temperature $^{31}P\{^1H\}$ NMR spectra were obtained under an N_2 atmosphere on a Bruker AC-300 spectrometer and referenced to 85% H_3PO_4 in D_2O as an external standard. The compositions of filtrate A from procedure 1 (eq 1) and the filtrate from procedure 2 (eq 2) were investigated after evaporation of each of these solutions in vacuum under liquid N_2 followed by complete dissolution of their dried residues in C_6D_6 under N_2; see Supporting Information. IR spectra were recorded on a Mattson Polaris Fourier transform IR spectrometer; Nujol suspensions were prepared under nitrogen. Coproducts were identified by X-ray diffraction determinations of the unit cell parameters and/or by IR and $^{31}P\{^1H\}$ NMR spectra. X-ray Au−Pd microanalyses were carried out by Dr. Richard Noll (Manager of the SEM Facility at the Materials Science Center, University of Wisconsin—Madison) on a field-emission scanning electron microscope (LEO 1530 FESEM) with an energy-dispersive detector.

*Synthesis of **1** via the Reaction of **5** with $Au(SMe_2)Cl$.* The following two-step synthetic pathway was utilized. A mixture of **5** (0.300 g, 0.142 mmol) and $Au(SMe_2)Cl$ (0.046 g, 0.156 mmol) in acetone (8 mL) and HOAc (0.5 mL) was stirred under N_2 in a 100 mL closed flask at 50 °C for 2 h. During the reaction, the atmosphere was refreshed by a N_2 flow (to remove emitted CO) after 10 and 90 min. The resulting black residue was filtered, washed with Me_2CO, and extracted with THF. Crystallization via vapor diffusion from a concentrated solution was set up under CO in the presence of a hexane/acetone (3:2) mixture in a 75 mL closed flask with a volume ratio of liquid/gas phases of 1:4. Black hexagonal platelike crystals of **1** (53 mg; 20% based on Pd, 13% based on Au) appeared slowly and were separated after 1 month of crystallization. Two major solutions (Figure 1s in the Supporting Information) were obtained from this procedure: namely, filtrate A collected under N_2 after treatment (50 °C, 2 h) of the original mixture (vide supra) and solution B, which resulted from the separation of crystals of **1** under CO. These solutions were examined as follows: the brown-yellow solution (A), kept under N_2 in the presence of vapors from 95% aqueous EtOH, gave ∼2 mg (<1%) of thin plates of $Pd_{34}(CO)_{24}(PEt_3)_{12}$[6k,l] and 30 mg (11%) of block crystals of $Pd_{16}(CO)_{13}(PEt_3)_9$.[6j] Further crystallization of this solution (A′), in the presence of CO and under vapors from 75% aqueous EtOH, afforded dark-red crystals of the expected **5** (20 mg, 6%) and a negligible amount of unidentified brown-red polycrystalline material. If the original solution A was kept under CO (instead of N_2) in the presence of vapors from 95% aqueous EtOH, it afforded dark-red crystals of **5** (52 mg, 17%) and black crystals of **3** (21 mg, 7%). On the other hand, without EtOH/H_2O vapors, it gave only crystals of **3** (14 mg, 4.7%) presumably because of kinetic/solubility effects. Evaporation of the red solution B to ∼3 mL and the subsequent addition of 10 mL of heptane expectedly gave crystals of **5** (24 mg, 8%). It should be noted that the Pd_{10} cluster **5** that was separated from both solutions A and/or A′ and B was not an initial product but instead one obtained from higher-nuclearity metal-cluster product(s) during crystallization under a CO atmosphere.

IR spectrum (Nujol) of **1**: ν(CO) 2028 (w-vw), 1911 (s), 1886 (s), 1860 (s), 1840 (m-w or sh), 1821 (sh), 1806 (sh), 1778 (w) cm^{-1}. $^{31}P\{^1H\}$ NMR spectrum of **1** in CD_2Cl_2 (121.4 MHz): δ 14.8 (s, br), 8.4 (s, br), 6.8 (s, br, 4P of equatorial PEt_3), 3.8 (s, br).

*Synthesis of **1** via the Reaction of **3** with **4**.* All procedures were performed under CO. A solution of an equimolar mixture of **3** (20 mg, 0.0046 mmol) and **4** (19.2 mg, 0.0046 mmol) in THF (3 mL) was stirred at room temperature for 15 min. The brown solution was filtered and crystallized under vapor diffusion from a hexane/acetone mixture (3:2). Even though this solution was considerably more dilute than the THF solution in the previous procedure, crystals of **1** appeared during the next day and were separated 2 weeks later as black elongated plates (8.4 mg; 22% based on Pd, 34% based on Au). IR spectrum (Nujol) of **1**: ν(CO) 2022 (w-vw), 1911 (s), 1886 (vs), 1860 (s), 1842 (sh), 1779 (w) cm^{-1}. A complete X-ray diffraction analysis, carried out on a single crystal from this reaction, revealed all crystallographic data to be virtually identical with those previously found for a crystal obtained from the two-step procedure, including the same location and similar electron density of the highest positive residual peak Q1 (vide infra).

An overall metal stoichiometry of **1** obtained from eq 2 was also substantiated by an X-ray Au−Pd field-emission microanalysis on two crystals with a scanning electron microscope. The calculated Au−Pd atom % ratio (Au_2Pd_{28}) of 6.7%/93.3% is in good agreement with that of 6.3%/93.7% and 7.0%/93.0% found for one crystal (with use of Au M and Au L lines, respectively) and with that of 7.8%/92.2% for a second crystal (Au L line).

*Reaction of **3** with **6**.* All procedures were carried out under CO. A solution of **3** (27.5 mg, 0.0063 mmol) and **6** (28.5 mg, 0.0046 mmol) in THF (3 mL) was stirred at room temperature for 30 min. The brown solution was filtered and crystallized under the same conditions as those described above for the reaction of **3** with **4**. After 2 weeks, thin elongated hexagonal plates of **1** (9.0 mg; 15% based on Pd, 27% based on Au) were separated. IR spectrum (Nujol) of **1**: ν(CO) 2026 (w-vw), 1911 (s), 1886 (vs), 1861 (s), 1840 (sh), 1776 (vw) cm^{-1}. Determination of the unit cell parameters by X-ray diffractometry at 100(2) K for one crystal gave the same monoclinic unit cell with experimentally equivalent parameters as those found for a crystal from the two-stage synthetic procedure.

*X-ray Crystallographic Determination of **1**.* A black hexagonal-shaped platelike crystal, obtained from the two-step equation (1) and cut into a block-shaped form of size 0.47 × 0.44 × 0.13 mm^3, was used for data collection. Intensity data were collected over an entire reciprocal lattice sphere at 100(2) K with a Bruker SMART CCD-1000 area detector system mounted on a Bruker P4 diffractometer with graphite-monochromated Mo Kα radiation from a sealed-tube generator. A multiscan absorption correction (*SADABS*) was applied [μ(Mo Kα) = 6.283 mm^{-1}; max/min transmission, 0.519/0.156]. The crystal structure was determined by the combined use of direct methods/difference Fourier syntheses together with least-squares refinement (based on F^2) carried out with *SHELXTL*:[38] $Au_2Pd_{28}P_{10}O_{26}C_{86}H_{150}$, M = 5283.52, monoclinic, $P2_1/n$, a = 18.982(1) Å, b = 17.257(1) Å, c = 19.674(1) Å, $\alpha = \gamma = 90°$, β = 94.834(1)°, V = 6421.7(6) $Å^3$, Z = 2, and ρ_{calcd} = 2.740 Mg/m^3. Mo Kα data were obtained at 100(2) K by 0.3ω scans over a 2θ range of 3.72−56.58°. Full-matrix least-squares refinement with all non-H atoms refined anisotropically and with all H atoms generated geometrically and refined as riding models (696 parameters; 0

restraints) on 15 760 independent reflections converged at wR2(F^2) = 0.053 for all data with R1(F) = 0.021 for $I > 2\sigma(I)$; GOF (on F^2) = 0.80; max/min residual electron density, +1.69/−0.85 e/Å^3. A structural CIF/PLATON test carried out by the http://journals.iucr.org/services/cif/checking/checkform.html service is in accordance with the crystal structure determination. The CCDC reference number is 711727. **1** has crystallographic $C_i(\bar{1})$ site symmetry, with the asymmetric part of the crystal structure consisting of half of the neutral cluster.

One salient crystallographic feature is that the structurally analyzed geometry of **1** determined from another crystal isolated from eq 2 was found to be virtually identical with that obtained from the crystal isolated from the two-step equation (1). In fact, both complete least-squares structural refinements clearly suggested the presence of two additional centrosymmetrically related tetracapped Pd atoms with identical site occupancies of $\alpha = 0.07$.[39] Because of this low-occupancy factor, we regard the presumed superimposed cocrystallized Au_2Pd_{30} cluster as a small impurity that can be neglected.

■ ASSOCIATED CONTENT

Supporting Information. Additional X-ray crystallographic data and experimental details for the reaction of **5** with $Au(SMe_2)Cl$, including a block diagram of synthetic step routes, reaction conditions, and resulting spectroscopically and/or crystallographically identified products. This material is available free of charge via the Internet at http://pubs.acs.org.

■ AUTHOR INFORMATION

Corresponding Author

*E-mail: mednikov@chem.wisc.edu (E.G.M.), dahl@chem.wisc.edu (L.F.D.).

■ ACKNOWLEDGMENT

This research was supported by the National Science Foundation, UOP LLC (Des Plaines, IL), and the University of Wisconsin—Madison (UW—Madison). The SMART 1000 CCD X-ray area detector system was purchased, in part, from NSF Grant CHE-9310428. The Bruker AC-300 NMR spectrometer was purchased, in part, by funds from NSF Grant CHE-9208963 and NIH Grant SIO RR 08389-01. This work was performed, in part, at the U.S. Department of Energy, Center for Integrated Nanotechnologies, at Los Alamos National Laboratory (Contract DE-AC52-06NA25396) and Sandia National Laboratories (Contract DE-AC04-94AL85000). Color and black-and-white structural drawings were prepared with *CrystalMaker* software (David C. Palmer, Centre for Innovation & Enterprise, Begbroke Science Park, Building 5, Sandy Lane, Yarnton, Oxfordshire OX5 1PF, U.K.). We are indebted to Professors Clark Landis and Frank Weinhold (UW—Madison) for their invaluable help to S.A.I. in the identification of particular program software errors initially encountered in the greatly enlarged DFT version required to provide massive number-crunching theoretical analyses of the nanosized metal-cluster systems. We are also grateful to Dr. Richard Noll (Materials Science Center, UW—Madison) for performing the X-ray Au−Pd microanalyses of **1** and to Dr. Ilia Guzei (UW—Madison) for use of the Departmental X-ray Crystallographic Facilities.

■ DEDICATION

Dedicated to Professor Dick Holm.

■ REFERENCES

(1) (a) Hutchings, G. J.; Brust, M.; Schmidbaur, H. *Chem. Soc. Rev.* **2008**, *37*, 1759. (b) Hutchings, G. J. *Chem. Commun.* **2008**, 1148 and references cited therein. (c) Hutchings, G. J. *Catal. Today* **2008**, *138*, 9. (d) Edwards, J. K.; Solsona, B.; Ntainjua, E. N.; Carley, A. F.; Herzing, A. A.; Kiely, C. J.; Hutchings, G. J. *Science* **2009**, *323*, 1037. (e) Edwards, J. K.; Ntainjua, E. N.; Carley, A. F.; Herzing, A. A.; Kiely, C. J.; Hutchings, G. J. *Angew. Chem., Int. Ed.* **2009**, *48*, 8512. (f) Gao, F.; Wang, Y.; Goodman, D. W. *J. Am. Chem. Soc.* **2009**, *131*, 5734. (g) Mertens, P. G. N.; Vandezande, P.; Ye, X.; Poelman, H.; De Vos, D. E.; Vankelecom, I. F. J. *Adv. Synth. Catal.* **2008**, *350*, 1241. (h) Hou, W.; Dehm, N. A.; Scott, R. W. J. *J. Catal.* **2008**, *253*, 22. (i) Zhou, Y.; Wang, S.; Ding, B.; Yang, Z. *Catal. Lett.* **2007**, *118*, 86. (j) Kesavan, L.; Tiruvalam, R.; Ab Rahim, M. H.; bin Saiman, M. I.; Enache, D. I.; Jenkins, R. L.; Dimitratos, N.; Lopez-Sanchez, J. A.; Taylor, S. H.; Knight, D. W.; Kiely, C. J.; Hutchings, G. J. *Science* **2011**, *331*, 195. (k) Lee, H. M.; Park, S. Y.; Park, K. T.; Jung, U.-H.; Chun, K.; Woong, C. D.; Kim, S. H. *Res. Chem. Intermed.* **2008**, *34*, 787.

(2) (a) Enache, D. I.; Edwards, J. K.; Landon, P.; Solsona-Espriu, B.; Carley, A. F.; Herzing, A. A.; Watanabe, M.; Kiely, C. J.; Knight, D. W.; Hutchings, G. J. *Science* **2006**, *311*, 362. (b) Chen, M.; Kumar, D.; Yi, C.-W.; Goodman, D. W. *Science* **2005**, *310*, 291 and references cited therein. (c) Sinfelt, J. H. *Bimetallic Catalysts*; Wiley: New York, 1983; Chapters 1 and 2. (d) Wacks, I. E. *Gold Bull.* **1983**, *16*, 98. (e) Schwank, J. *Gold Bull.* **1985**, *18*, 1. (f) Alexander, B. D.; Gomez-Sal, M. P.; Gannon, P. R.; Blaine, C. A.; Boyle, P. D.; Mueting, A. M.; Pignolet, L. H. *Inorg. Chem.* **1988**, *27*, 3301. (g) Mueting, A. M.; Bos, W.; Alexander, B. D.; Boyle, P. D.; Casalnuovo, J. A.; Balaban, S.; Ito, L. N.; Johnson, S. M.; Pignolet, L. H. *New J. Chem.* **1988**, *12*, 505. (h) Pignolet, L. H.; Aubart, M. A.; Craighead, K. L.; Gould, R. A. T.; Krogstad, D. A.; Wiley, J. S. *Coord. Chem. Rev.* **1995**, *143*, 219. (i) Krogstad, D. A.; Konze, W. V.; Pignolet, L. H. *Inorg. Chem.* **1996**, *35*, 6763. (j) Jones, P. G. *Gold Bull.* **1986**, *19*, 46. (k) Toshima, N.; Yonezawa, T. *New J. Chem.* **1998**, *22*, 1179. (l) Horvath, I. T. *Encyclopedia of Catalyses*; Wiley-Interscience: New York, 2003; Vol. 1, pp 621−665. (m) Braunstein, P.; Rose, J. In *Stereochemistry of Organometallic and Inorganic Compounds*; Bernal, I., Ed.; Elsevier: Tarrytown, NY, 1998; Vol. 3. (n) Ichikawa, M. *Adv. Catal.* **1992**, *38*, 283 and references cited therein. (o) *Catalysis by Di- and Polynuclear Metal Cluster Complexes*; Adams, R. D., Cotton, F. A., Eds.; Wiley-VCH: New York, 1998. (p) Mingos, D. M. P.; Watson, M. J. *Adv. Inorg. Chem.* **1992**, *39*, 327 and references cited therein. (q) Hashmi, A. S. K.; Lothschütz, C.; Döpp, R.; Rudolph, M.; Ramamurthi, T. D.; Rominger, F. *Angew. Chem., Int. Ed.* **2009**, *48*, 8243. (r) Hirner, J. J.; Shi, Y.; Blum, S. A. *Acc. Chem. Res.* **2011**, *44*, 603 and references cited therein.

(3) (a) Ito, L. N.; Johnson, B. J.; Mueting, A. M.; Pignolet, L. H. *Inorg. Chem.* **1989**, *28*, 2026. (b) Ito, L. N.; Felicissimo, A. M. P.; Pignolet, L. H. *Inorg. Chem.* **1991**, *30*, 988.

(4) (a) Laupp, M.; Strähle, J. *Z. Naturforsch., Teil B* **1995**, *50*, 1369. (b) Laupp, M.; Strähle, J. *Angew. Chem., Int. Ed. Engl.* **1994**, *33*, 207.

(5) Copely, R.; Hill, C. M.; Mingos, D. M. P. *J. Cluster Sci.* **1995**, *6*, 71.

(6) (a) Tran, N. T.; Powell, D. R.; Dahl, L. F. *J. Chem. Soc., Dalton Trans.* **2004**, 209. (b) Tran, N. T.; Powell, D. R.; Dahl, L. F. *J. Chem. Soc., Dalton Trans.* **2004**, 217. (c) Mednikov, E. G.; Tran, N. T.; Aschbrenner, N. L.; Dahl, L. F. *J. Cluster Sci.* **2007**, *18*, 253. (d) Mednikov, E. G.; Dahl, L. F. *J. Cluster Sci.* **2005**, *16*, 287. (e) Mednikov, E. G.; Wittayakun, J.; Dahl, L. F. *J. Cluster Sci.* **2005**, *16*, 429 and references cited therein. (f) Mednikov, E. G.; Eremenko, N. K.; Slovokhotov, Yu. L.; Struchkov, Yu. T. *J. Organomet. Chem.* **1986**, *301*, C35. (g) Mednikov, E. G.; Ivanov, S. A.; Dahl, L. F. *Angew. Chem., Int. Ed.* **2003**, *42*, 323. (h) Ivanov, S. A.; de Silva, N.; Kozee, M. A.; Nichiporuk, R. V.; Dahl, L. F. *J. Cluster Sci.* **2004**, *15*, 233. (i) Tran, N. T.; Kawano, M.; Dahl, L. F. *J. Chem. Soc., Dalton Trans.* **2001**, 2731. (j) Mednikov, E. G.; Slovokhotov, Yu. L.; Struchkov, Yu. T. *Metalloorg. Khim.* **1991**, *4*, 123 [*Organomet. Chem. USSR* **1991**, *4*, 65 (Engl. Transl.)]. (k) Belyakova, O. A.; Slovokhotov, Yu. L. *Russ. Chem. Bull.* **2003**, *52*, 2299 (Engl. Transl.). (l) Mednikov, E. G.; Kanteeva, N. I. *Izv. Acad. Nauk, Ser. Khim.* **1995**, 167 [*Russ. Chem. Bull.* **1995**, *44*, 163 (Engl. Transl.)]. (m) Mednikov, E. G.; Eremenko, N. K. *Izv. Acad. Nauk SSSR, Ser. Khim.* **1982**, 2540 [*Bull. Acad. Sci. USSR,*

Div. Chem. Sci. **1982**, *31*, 2240 (Engl. Transl.)]. (n) Mednikov, E. G.; Eremenko, N. K. *Izv. Acad. Nauk SSSR Ser. Khim.* **1984**, 2781 [*Bull. Acad. Sci. USSR, Div. Chem. Sci.* **1984**, *33*, 2547 (Engl. Transl.)]. (o) Mednikov, E. G.; Eremenko, N. K.; Slovokhotov, Yu. L.; Struchkov, Yu. T. *Zh. Vses. Khim. O-va. im. D. I. Mendeleeva* **1987**, *32*, 101 (in Russian). (p) Mednikov, E. G. *Izv. Akad. Nauk SSSR, Ser. Khim.* **1993**, 1299 [*Russ. Chem. Bull.* **1993**, *42*, 1242 (Engl. Transl.)]. (q) Mednikov, E. G.; Ivanov, S. A.; Wittayakun, J.; Dahl, L. F. *J. Chem. Soc., Dalton Trans.* **2003**, 1686. (r) Mednikov, E. G.; Dahl, L. F. *J. Chem. Educ.* **2009**, *86*, 1135. (s) Mednikov, E. G. *Metalloorg. Khim.* **1991**, *4*, 1237 [*Organomet. Chem. USSR* **1991**, *4*, 608 (Engl. Transl.)]. Mednikov, E. G.; Kanteeva, N. I. Unpublished research, 1991−1995. (t) Mednikov, E. G.; Eremenko, N. K.; Slovokhotov, Yu. L.; Struchkov, Yu. T. *J. Chem. Soc., Chem. Commun.* **1987**, 218. (u) Mednikov, E. G.; Eremenko, N. K.; Slovokhotov, Yu. L.; Struchkov, Yu. T.; Gubin, S. P. *J. Organomet. Chem.* **1983**, *258*, 247. (v) Kawano, M.; Bacon, J. W.; Campana, C. F.; Winger, B. E.; Dudek, J. D.; Sirchio, S. A.; Scruggs, S. L.; Geiser, U.; Dahl, L. F. *Inorg. Chem.* **2001**, *40*, 2554. (w) Mednikov, E. G.; Dahl, L. F. Unpublished research, 2001. (x) Tran, N. T.; Kawano, M.; Powell, D. R.; Dahl, L. F. *J. Am. Chem. Soc.* **1998**, *120*, 10986.

(7) Two other octahedrally based $Pd_{23}(CO)_x(PEt_3)_{10}$ clusters containing $Pd_{23}P_{10}$ fragment geometries essentially equivalent to that of **4**[6e] but additionally possessing one extra ($x = 21$)[6e] or two extra ($x = 22$)[6f] CO ligands coordinated to the analogous octahedral metal-core faces of **4** have been isolated and crystallographically characterized. These three variable carbonyl $Pd_{23}(CO)_x(PEt_3)_{10}$ clusters (with $x = 20$,[6e] 21,[6e] and 22[6f]) were generated via fragmentation/growth processes from solutions of the $Pd_{10}(CO)_{12}(PEt_3)_6$ precursor (**5**) under N_2 with/without the assistance of any other reagents. Their observed structures with variable CO coverage may be viewed to represent X-ray snapshots of the dynamic behavior of chemisorbed CO molecules on pseudonanosized octahedral Pd(111) faces.

(8) Mednikov, E. G.; Dahl, L. F. *Philos. Trans. R. Soc. A* **2010**, *368*, 1301.

(9) (a) The acetone-solvated **2** was obtained in low yields (<5%) from room temperature reactions of **5** with CF_3CO_2H or CF_3CO_2H/HOAc in Me_2CO/*i*-Pr_2O or Me_2CO/Et_2O solutions with a short-time (1−2 h) treatment under a CO atmosphere.[6g] It should be emphasized that this synthetic procedure leading to **2** *always necessitates time-restricted exposure under a CO atmosphere*, whereas the preparations of other homopalladium $Pd_n(CO)_x(PR_3)_y$ clusters ($n > 10$) normally do not require CO assistance.

(10) Marks, L. D. *Rep. Prog. Phys.* **1994**, *57*, 603 and references cited therein.

(11) Donohue, J. *The Structure of the Elements*; John Wiley & Sons: New York, 1974: Pd, p 216; Au, p 222.

(12) Frisch, M. J.; Trucks, G. W.; Schlegel, H. B.; et al. *Gaussian 09*, revision A.1; Gaussian, Inc.: Wallingford, CT, 2009.

(13) Becke, A. D. *J. Chem. Phys.* **1993**, *98*, 5648.

(14) Perdew, J. P.; Burke, K.; Wang, Y. *Phys. Rev. B* **1996**, *54*, 16533.

(15) Hay, P. J.; Wadt, W. R. *J. Chem. Phys.* **1985**, *82*, 270 and 299.

(16) Check, C. E.; Faust, T. O.; Bailey, J. M.; Wright, B. J.; Gilbert, T. M.; Sunderlin, L. S. *J. Phys. Chem. A* **2001**, *105*, 8111.

(17) Hehre, W. J.; Ditchfield, R.; Pople, J. A. *J. Chem. Phys.* **1972**, *56*, 2257.

(18) Reed, A. E.; Weinstock, R. B.; Weinhold, F. *J. Chem. Phys.* **1985**, *83*, 735.

(19) Relative electronegativity values based upon different scales[20] show Au metal to be considerably more electronegative than Pd metal. A striking illustration of this difference (which can be correlated with the degree of heterometallic ionic character) is given by the remarkable geometrical variation between the central face-fused $(\mu_{13}\text{-Au})_2Pd_{29}$ fragment of the Au_2Pd_{41} core in $Au_2Pd_{41}(CO)_{27}(PEt_3)_{15}$[6b] and the corresponding central $(\mu_{12}\text{-Pd})_2Pd_{27}$ fragment of the Pd_{35} core in $Pd_{35}(CO)_{23}(PMe_3)_{15}$;[6i] this 13-atom coordination of each central Au atom versus the closely related 12-atom coordination of each analogous central Pd atom was attributed[6b] to a large induced electronegativity Au−Pd mismatch in radial bonding due to the replacement of each Pd-centered atom with a more electronegative Au-centered atom (i.e., Au has been considered as the most electronegative metal).

(20) (a) Pauling, L. *J. Am. Chem. Soc.* **1931**, *53*, 1367.Pauling, L. *The Nature of the Chemical Bond*, 3rd ed.; Cornell University Press: Ithaca, NY, 1960. (b) Allred, A. L. *J. Inorg. Nucl. Chem.* **1961**, *17*, 215. (c) Allen, L. C. Electronegativity and the Periodic Table. In *The Encyclopedia of Computational Chemistry*; Schleyer, P. v. R., Allinger, N. L., Clark, T., Gasteiger, J., Kollman, P. A., Schaefer, H. F., III, Schreiner, P. R., Eds.; Wiley: Chichester, U.K., 1998. (d) Pearson, R. G. *Chemtracts: Inorg. Chem.* **1991**, *3*, 317.

(21) (a) Wiberg, K. A. *Tetrahedron* **1968**, *24*, 1083. (b) Sizova, O. V.; Skripnikov, L. V.; Sokolov, A. Yu.; Sizov, V. V. *Int. J. Quantum Chem.* **2009**, *109*, 2581 and references cited therein.

(22) Ames, L. L.; Barrow, R. F. *Trans. Faraday Soc.* **1967**, *63*, 39.

(23) (a) A dramatic example of the resulting additional ligation of the naked Au_2 dimer producing a larger Au−Au distance due to increased delocalization of the Au 6s electrons is given by the crystal structure of $[Au_2Pt_2(dmb)_2(PPh_3)_4)]^{2+}$ as the $[PF_6]^-$ salt (where dmb denotes 1,8-diisocyano-*p*-menthane). This Au−Pt cluster, prepared and crystallographically characterized by Harvey and co-workers,[23b] contains a quasi-linear $Ph_3PAu-AuPPh_3$ fragment encapsulated inside a 20-membered interlocking $[Pt_2(dmb)_2]^{2+}$ ring system; its trigonal-planar-like coordination of an axial PPh_3 and two symmetrically bridging Pt^I to each Au gives rise to a 0.13-Å-longer Au−Au bond of 2.598(1) Å, which primarily occurs via increased Au 6s delocalization (donation) to the two Pt^I atoms from the filled Au−Au σ_g bonding orbital, which is also lengthened by PPh_3-induced orbital hybridization. The resulting Au−Au interaction was described[23b] as a strong formal Au^0-Au^0 single bond on the basis of the cluster's spectral properties including it being luminescent at room temperature in the solid state. A virtually identical Au−Au distance of 2.593(2) Å was previously reported by Mingos and co-workers[23c] for the analogous isocyanide $[Au_2Pt_2(CNR)_4(PPh_3)_4]^{2+}$ cluster (R = 2,6-$Me_2C_6H_3$) as the $[PF_6]^-$ salt; however, the observed asymmetry in the Pt−Au bond lengths with both bridging Pt atoms being 0.2 Å closer to one Au atom led Gilmour and Mingos[23d] to propose a different bonding description. Nevertheless, Mingos and co-workers[23c] pointed out that $^{31}P\{^1H\}$ NMR studies also suggested that their monodentate isocyanide Au_2Pt_2 cluster in solution adopts a symmetric D_{2h} structure (with a linear PAu−AuP geometry) in which the Au atoms are equivalent. (b) Zhang, T.; Drouin, M.; Harvey, P. D. *Inorg. Chem.* **1999**, *38*, 4928. (c) Briant, C. E.; Gilmour, D. I.; Mingos, D. M. P. *J. Chem. Soc., Dalton Trans.* **1986**, 835. (d) Gilmour, D. I.; Mingos, D. M. P. *J. Organomet. Chem.* **1986**, *302*, 127.

(24) (a) This terminology, which was coined in 1989 by Schmidbauer,[24b−d] is utilized to denote Au−Au connectivities among closed-shell Au^I centers at distances of 2.7−3.3 Å; these attractive interactions have been ascribed from extensive experimental evidence[24b−d] and theoretical studies by Pyykko[25] to strong dispersion forces (also described as correlation effects) that are markedly enhanced by relativistic effects, which are particularly pronounced for gold. (b) Schmidbaur, H. *Chem. Soc. Rev.* **1995**, *24*, 391. (c) Schmidbaur, H. *Gold Bull.* **2000**, *33*, 3. (d) Schmidbaur, H.; Cronje, S.; Djordjevic, B.; Schuster, O. *Chem. Phys.* **2005**, *311*, 151. (e) Schmidbaur, H.; Schier, A. *Chem. Soc. Rev.* **2008**, *37*, 1931.

(25) (a) Pyykko, P. *Angew. Chem., Int. Ed.* **2004**, *43*, 4412. (b) Pyykko, P. *Inorg. Chim. Acta* **2005**, *358*, 4113. (c) Pyykko, P. *Chem. Soc. Rev.* **2008**, *37*, 1967.

(26) (a) Mednikov, E. G.; Eremenko, N. K.; Mikhailov, V. A.; Gubin, S. P.; Slovokhotov, Yu. L.; Struchkov, Yu. T. *J. Chem. Soc., Chem. Commun.* **1981**, 989. (b) Mednikov, E. G.; Eremenko, N. K.; Gubin, S. P.; Slovokhotov, Yu. L.; Struchkov, Yu. T. *J. Organomet. Chem.* **1982**, *239*, 401. (c) Mingos, D. M. P.; Hill, C. M. *Croat. Chem. Acta* **1995**, *68*, 745.

(27) Use of the Au^I precursor, $Au(SMe_2)Cl$, also played a crucial role in obtaining **1** from eq 1; thus, the alternative use of PPh_3-containing $Au(PPh_3)Cl$ produced the Au_2Pd_{21} cluster **3** instead of **1**.

(28) The finding of the mononuclear Pd^{II} complex $Pd(PEt_3)_2Cl_2$ in the original filtrate was expected; its formation is invariably observed in a considerable number of reactions between palladium carbonyl/

phosphine clusters (e.g., Pd_{10} **5**, $Pd_{23}P_{10}$ **4**) and gold precursors [e.g., $Au(SMe_2)Cl$, $Au(PPh_3)Cl$],[27] when performed under different acidic/basic conditions with different solvents and at various temperatures. The detection of this mononuclear square-planar Pd^{II} complex indicates that at least part of the Au^I precursor was reduced by zerovalent Pd atoms of the Pd_{10} **5** precursor. Another favorable pathway of Au^I reduction is by CO (which readily originates from the Pd_{10} reactant) and traces of water. These conclusions are consistent with the absence in the original filtrate of the nonreduced Au^I coproduct, namely, $Au(PEt_3)Cl$,[29] which suggests that all of the gold initially in $Au(SMe_2)Cl$ had been reduced.

(29) A $^{31}P\{^1H\}$ NMR spectrum of $Au(PEt_3)Cl$ in a C_6D_6 solution displayed a single phosphorus resonance at 30.3−30.1 ppm. Upon the addition of 0.7 equiv of free PEt_3 ligand up to a total Au/PEt_3 ratio of 1:1.7, the resultant $^{31}P\{^1H\}$ NMR signal broadened, and its chemical shift moved downfield to 35.6 ppm.

(30) The most common isolated product of all continued reactions under a CO atmosphere was the cluster **5**.[26] In fact, Pd_{10} and the "butterfly" $Pd_4(CO)_5(PR_3)_4$ clusters[31] are the two most stable clusters in the CO/PR_3-ligated Pd_n family (R = Et, Bu^n, Ph) under an *unrestricted* CO atmosphere.[6m,n]

(31) (a) Dubrawski, J.; Kriege-Simondsen, J. C.; Feltham, R. D. *J. Am. Chem. Soc.* **1980**, *102*, 2089. (b) Mednikov, E. G.; Eremenko, N. K.; Slovokhotov, Yu. L.; Struchkov, Yu. T.; Gubin, S. P. *Koord. Khim.* **1987**, *13*, 979 [*Sov. J. Coord. Chem.* **1987**, *13*, 554 (Engl. Transl.)].

(32) Belli Dell'Amico, D.; Labella, L. *J. Organomet. Chem.* **2000**, *593*−*594*, 427.

(33) (a) Darling, J. H.; Ogden, J. S. *Inorg. Chem.* **1972**, *11*, 666. (b) Kündig, E. P.; Moskovits, M.; Ozin, G. A. *Can. J. Chem.* **1972**, *50*, 3587. (c) Huber, H.; Kündig, E. P.; Moskovits, M.; Ozin, G. A. *Nat. Phys. Sci.* **1972**, *235*, 98.

(34) Ciani, G.; Sironi, A. *J. Organomet. Chem.* **1980**, *197*, 233.

(35) (a) Mingos, D. M. P. *Acc. Chem. Res.* **1984**, *17*, 311. (b) Mingos, D. M. P. *Polyhedron* **1984**, *3*, 1289. (c) Hall, K. P.; Mingos, D. M. P. *Prog. Inorg. Chem.* **1984**, *32*, 237. (d) Mingos, D. M. P.; Johnson, R. L. *J. Organomet. Chem.* **1985**, *281*, 419. (e) Mingos, D. M. P.; Zhenyang, L. *J. Chem. Soc., Dalton Trans.* **1988**, 1657 and references cited therein. (f) Mingos, D. M. P.; May, A. P. In *The Chemistry of Metal Cluster Complexes*; Shriver, D. F., Kaesz, H. D., Adams, R. D., Eds.; VCH Publishers: New York, 1990; Chapter 2, pp 11−119.

(36) Teo, B. K.; Zhang, H. *Polyhedron* **1990**, *9*, 1985. (b) Teo, B. K.; Sloane, N. J. *Inorg. Chem.* **1986**, *25*, 2315.

(37) Gu, X.; Lu, Z.-H.; Jiang, H.-L.; Akita, T.; Xu, Q. *J. Am. Chem. Soc.* **2011**, *133*, 11822.

(38) Sheldrick, G. All crystallographic software and sources of the scattering factors are contained in: *SHELXTL Program Library*, version 6.10; Bruker Analytical X-ray Systems: Madison, WI, 2000.

(39) The initial least-squares refinement of cluster **1** revealed the highest residual peak Q1 on the final difference map to possess an electron density of 10.3 e/Å^3, whereas that for the second highest peak was only 1.7 e/Å^3. Analogous residual peaks of 11.0 and 1.8 e/Å^3, respectively, were obtained from a corresponding final difference map of another complete structural determination of **1** based upon a crystal obtained from the one-step direct reaction of Au_2Pd_{21} **3** with Pd_{23} **4**. In both refinements, the highest Q1 peak and its centrosymmetrically equivalent one were found to occupy the two remaining "open" square faces of the Au_2Pd_{28} kernel in **1** (see Figure 1a) within a reasonable range of Pd−Pd distances (2.7−3.0 Å). Additional refinements of the two virtually identical structures of **1** based upon the assignment of Q1 as an independent Pd(15) atom gave rise to identical occupancy factors of α = 0.07 with resulting reasonable Pd(15)−Pd distances to the adjacent square-capped Pd and wingtipped Pd(exo) atoms of 3.0−3.3 Å. Additional ligand atoms connected to Pd(15) were expectedly not detected on subsequent difference maps because of their much smaller X-ray scattering powers. Normally, Pd atoms that cap square Pd_4 faces in palladium CO/PR_3-ligated clusters possess P atoms. However, in the case of the Pd(15) atom, this possibility was ruled out because a hypothetical Pd(15)−P bond, which should be approximately collinear with the analogous neighboring square-capped Pd−P bond in **1**, would result in a nonbonding P−P separation being too close (<3.2 Å) and thereby would be sterically impossible upon the addition of its three triethylphosphine substituents. Hence, we consider that the independent Pd(15) atom is most likely coordinated to a terminal CO ligand, which is in accordance with a weakly characteristic band of 2028−2022 cm^{-1}, which was observed in Nujol IR spectra of **1**. Although terminal coordination of a CO ligand is not common for palladium CO/PR_3-ligated clusters, this kind of linkage was previously determined from X-ray diffraction studies of $Pd_{10}(CO)_2(\mu_2\text{-}CO)_8(\mu_3\text{-}CO)_4(PBu^n{}_3)_4$,[6u] which has a terminal CO attached to each of the two apical Pd atoms and of the isostructural $[Pd_{16}Ni_4(CO)_{22}(PR_3)_4]^{2-}$ dianions (R = Ph,[6v] Et[6w]), in which a terminal CO is linked to the Pd atom capping each of the four tetrahedral faces of the central ν_3 $Pd_{16}Ni_4$ tetrahedron. The coordinative stability of the Pd(15) atom can also be achieved through possible triply bridging ligation with one or both of the doubly bridging CO ligands that edge-bridge opposite sides of the two centrosymmetrically unoccupied (open) Pd_4 square faces in **1**. A similar situation was previously encountered in the crystal structure of $Pd_{59}(CO)_{32}(PMe_3)_{21}$,[6x] where a refinement detected the existence of an additional Pd atom (with partial occupancy of α = 0.04) in the asymmetric unit (along with five other symmetry-related Pd atoms). This indication of a superimposed cocrystallized Pd_{65} cluster of $D_3(32)$ site symmetry occupying ∼4% of the unit cells was likewise regarded as a small impurity that could be neglected.